T.C.
İSTANBUL UNIVERSITY
INSTITUTE OF GRADUATE STUDIES IN
SCIENCE AND ENGINEERING

M.Sc. THESIS

EXPERIMENTAL FTIR INVESTIGATION OF VIBRATIONAL SPECTRA OF A COPPER-PROTHIONAMIDE COMPLEX

Somaeia Mohamed ADARRAT

Department of Physics

Physics Programme

SUPERVISOR
Assoc. Prof. Dr. Ayberk YILMAZ

June, 2018

İSTANBUL

This study was accepted on 8/6/2018 as a M. Sc. thesis in Department of Physics, Physics Programme by the following Committee.

Examining Committee Members

Assoc. Prof. Dr. Ayberk YILMAZ(Supervisor)
İstanbul University
Faculty of Science

Prof. Dr. Bayram DEMİR
İstanbul University
Faculty of Science

Assoc. Prof. Dr. Olcay Bölükbaşı
YALÇINKAYA
İstanbul University
Faculty of Science

Assist. Prof. Dr. Fatma Aydoğmuş ŞEN
İstanbul University
Faculty of Science

Assist. Prof. Dr. Serpil ÇIKIT
Haliç University
Faculty of Arts and Scieces

As required by the 9/2 and 22/2 articles of the Graduate Education Regulation which was published in the Official Gazette on 20.04.2016, this graduate thesis is reported as in accordance with criteria determined by the Institute of Graduate Sttudies in Science and Engineering by using the plagiarism software to which İstanbul University is a subscriber.

FOREWORD

I would like to express my gratitude to my several excellent advisors. First, I would like to thank my supervisor Assoc. Prof. Dr. Ayberk YILMAZ for guidance with respect to my personal career development.

I would like to thank my committee member: Prof. Dr. Bayram Demir and I express my thanks and appreciation to Prof. Dr. Mustafa Kumru.

Lastly, I want to thank my family for all the years of encouragement and support.

June 2018 Somaiea Mohamed ADARRAT

TABLE OF CONTENTS

Page

FOREWORD .... **iv**
TABLE OF CONTENTS .... **v**
LIST OF FIGURES .... **vii**
LIST OF TABLES .... **viii**
LIST OF SYMBOLS AND ABBREVIATIONS .... **ix**
ÖZET .... **xi**
SUMMARY .... **xii**
1. INTRODUCTION **1**
2. MATERIALS AND METHODS **3**
  2.1. SPECTROSCOPY 3
  2.2. ELECTROMAGNETIC RADIATION 3
  2.3. INFRARED SPECTROSCOPY 5
    2.3.1. The Vibrational Energy Of Diatomic Molecule 5
    2.3.2. Fundamental Vibrations 8
    2.3.3. IR Absorption Process 8
    2.3.4. IR Regions 9
  2.4. FOURIER TRANSFORM IR SPECTROMETER 10
    2.4.1. Basic Integral Equation 12
    2.4.2. The Michelson Interferometer 13
    2.4.3. Attenuated Total Reflectance (ATR) 14
    2.4.4. ATR Mechanism 16
  2.5. HARTREE FOCK APPROACH 17
    2.5.1. Born–Oppenheimer Approach 17
    2.5.2. AB Initio Method 19
  2.6. DENSITY FUNCTIONAL THEORY 19
    2.6.1. Basis Sets 21
    2.6.2. Gaussian Program 21
  2.7. GEOMETRY OPTIMIZATION 22
  2.8. VIBRATIONAL FREQUENCIES 23
  2.9. TRANSITION METAL COMPLEX 25

2.10. NORMAL COORDINATES 26
2.11. INTERNAL COORDINATES 27
3. RESULTS 28
4. DISCUSSION 40
5. CONCLUSION AND RECOMMENDATIONS 42
REFERENCES 43
CURRICULUM VITAE 46

LIST OF FIGURES

Page

Figure 2.1: Electromagnetic spectrum......4

Figure 2.2: Infrared region. 5

Figure 2.3: Diatomic molecule. 6

Figure 2.4: Harmonic oscillator and anharmonic oscillator. 7

Figure 2.5: Molecular motions. 8

Figure 2.6: Michelson interferometer. 13

Figure 2.7: ATR Single reflection. 16

Figure 2.8: Potential energy curves. 18

Figure 2.9: Nuclear reaction. 19

Figure 2.10: Single point Hartree-Fock energies for water molecule. 22

Figure 2.11: Molecular geometry vs. HF energy. 23

Figure 2.12: Vibrations of methylene group in a molecule. 27

Figure 3.1: Optimized geometry of the complex......28

Figure 3.2: Calculated IR spectrum of the complex. 39

Figure 3.3: FT-IR spectrum of the complex......39

LIST OF TABLES

Page

Table 2.1: Examples of coordination complex. 25

Table 2.2: Details of six internal coordinates. 27

Table 3.1: Optimized geometry of the complex. 29

Table 3.2: Comparison of the experimental wavenumbers (cm^{-1}) and theoretical harmonic wavenumbers (cm^{-1}) of the complex calculated by B3LYP with 6-31G(d,p) basis set 32

LIST OF SYMBOLS AND ABBREVIATIONS

Symbol	**Explanation**
ϖ	: Oscillation Frequency
χ_e	: Corresponding Anharmonicity Constant
K	: Spring Constant
M	: Mass
X	: Displaced Vector of Mass
O_2	: Dioxygen
NO	: Nitric Oxide
$\bar{\nu}$	: Wavenumber
v	: Frequency
c	: Speed of Light
E	: Electric Field
H	: Magnetic Field
ν	: Stretching
δ	: In Plane Bending
γ	: Out of Plane Bending
τ	: Torsion

Abbreviation	**Explanation**
ATR	: Attenuated total reflectance
B3LYP	: Becke’s Three Parameter Exchange Functional Combined with Lee-Yang-Parr Correlation Functional
BO	: Born Oppenheimer
DFT	: Density Functional Theory
FT	: Fourier Transform
FTIR	: Fourier Transform Infrared Spectroscopy
HF	: Hartree-Fock
IR	: Infrared
PED	: Potential Energy Distributions
QCD	: Quantum Chromo Dynamics

ÖZET

YÜKSEK LİSANS TEZİ

BAKIR-PROTİONAMİD KOMPLEKSİNİN TİTREŞİM SPEKTRUMUNUN DENEYSEL FTIR İNCELENMESİ

Somaiea Mohamed ADARRAT

İstanbul Üniversitesi

Fen Bilimleri Enstitüsü

Fizik Anabilim Dalı

Danışman : Doç. Dr. Ayberk YILMAZ

Bu tezde, Protiyonamid'in ($CuCl_2$(PTH); PTH = Prothionamide) Bakır(II) klorür kompleksinin moleküler yapısı ve titreşim spektrumları Yoğunluk Fonksiyonel Teorisi (DFT) ile araştırılmıştır. Kompleksin geometri optimizasyonu ve titreşimsel dalgasayısı hesaplamaları, Yoğunluk Fonksiyonel Teorisi(DFT), B3LYP fonksiyoneli ile 6-31G(d,p) baz kümesi kullanılarak gerçekleştirilmiştir. Hesaplanan dalgasayıları 0.961'lik bir faktörle ölçeklendirildi. Kompleksin teorik olarak tahmin edilen IR spektrumları oluşturuldu. Kompleksin titreşim spektrumunun yorumlanması, PED yardımıyla gerçekleştirilmiştir. Kompleksin FTIR spektrumu oda sıcaklığında 4000-600 cm^{-1} aralığında kaydedildi. Teorik olarak öngörülen IR spektrumu ve deneysel FTIR spektrumunun iyi bir uyum içinde olduğu görülmüştür.

Haziran 2018, 58. sayfa.

Anahtar kelimeler: Titreşim spektroskopisi, Protioamid, DFT, Metal kompleksi

SUMMARY

M.Sc. THESIS

EXPERIMENTAL FTIR INVESTIGATION OF VIBRATIONAL SPECTRA OF A COPPER-PROTHIONAMIDE COMPLEX

Somaiea Mohamed ADARRAT

İstanbul University

Institute of Graduate Studies in Science and Engineering

Department of Physics

Supervisor : Assoc. Prof. Dr. Ayberk YILMAZ

In this thesis, the molecular structure and vibrational spectra of Copper(II) chloride complex of prothionamide (CuCl2(PTH); PTH=Prothionamide) were investigated by Density Functional theory(DFT). The geometry optimization and vibrational wavenumber calculations of the complex were performed by Density Functional Theory (DFT) using B3LYP functional with 6-31G (d,p) basis set. The calculated wavenumbers were scaled by a factor of 0.961. The theoretically predicted IR spectra of the complex were constructed. Interpretation of the vibrational spectrum of the complex was carried out with aid of PED. An FTIR spectrum of the complex was recorded at room temperature in the range of 4000–600 cm^{-1}. The theoretically predicted IR spectrum and experimental FTIR spectrum were seen to be in good agreement.

June 2018, 58. pages.

Keywords: Vibrational Spectroscopy, Prothionamide, DFT, Metal Complex

1. INTRODUCTION

Complex compounds are composed of a central metal cation and various anions and / or molecules attached called ligands. It is known that transition metal complexes of some drug molecules have antibacterial, antifungal, antimicrobial, antiulcer, anticancer, antitumor and widely antioxidant properties. The importance of coordination compounds in biological processes is known. The complexes in which the metal ions are introduced into the biological structure by the pyrrole system are biological catalysts (Bernheim&Bernheim, 1931).

In recent years, it has become increasingly important to study the structure and the properties of complex compounds which are generated by transition metals and drug molecules. Metal complexes are used as complementary therapeutic agents, which are essential for the discovery, design and optimization of new, effective and safe drugs. Coordination compounds have many uses in medicine and pharmacology.

Prothionamide molecule is among the secondary drugs used to treat tuberculosis and to strengthen the immune system against tuberculosis. Its chemical formula is C9H12N2S Its molecular weight is 180.27 g/mol (Janin, 2007; Fajardo et al., 2006). Its appearance is yellow crystals or crystalline solid Prothionamide is insoluble in water and it is well soluble in alcohol well.

In the treatment of tuberculosis; drug resistance, the length of the treatment duration, the precise knowledge of the drugs effect mechanism and the toxic effects of the drugs on the body are important issues in terms of medicine and pharmacology. In the new drug discovery process, the molecular interactions at the molecular level are needed to be fully known. Copper complexes of drug molecules are intresting because of their reduction potential (James & Williams, 1961).

In this thesis, the optimized geometry of the copper complex of prothionamide, vibrational modes and wavenumbers are calculated by density functional theory (DFT) using B3LYP functional with 6-31G(d,p) basis set using Gaussian program (Gaussian 09, Revision A.02, Gaussian Inc., Wallingford CT, 2009). The vibrational modes are determined using potential energy distributions (PED) (Pulay&T’drilk, 1967; Keresztury&Jalsovszky, 1971). The

GAR2PED program(Martin, J.M.L. and A.C. Van, GAR2PED, 1995) was used to calculate the PED values. Theoretical IR simulation spectrum is plotted. A factor of 0.965(CCCBDB, 2018) was used when scaling the calculated wavenumbers. The calculated wavenumber were compared with the experimental values. Jmol program (Jmol, version 13.0, 2018) was used to visualization of molecular structure.

2. MATERIALS AND METHODS

2.1. SPECTROSCOPY

The interaction between electromagnetic radiation and matter is called the study of spectroscopy. In historical context, the study of visible light dispersion rendering the wavelength through a prism led to originate the spectroscopy. However, the concept has greatly evolved later and expanded to any radiative energy interaction which be the function of its respective wavelength. The emission spectrum provides representation of the spectroscopic data in the form of a plot that contains response of interest which represents the function of wavelength.

Therefore, spectroscopy refers to the measurement of intensity of radiation which is a function of wavelength or frequency and experimental spectroscopic methods are well described consequently. There are several spectral devices of measurement e.g., spectral analysers, spectrophotometers, and spectrometers. It is pertinent to mention here that spectroscopy can also be related to everyday observations of color. Moreover, the direction of application of atomic spectroscopy is “Neon lighting” Neon along with other “noble gases” possesses the characteristics of emission frequency (colors) (Kavan&Kastner, 1999). Neon lamps excite these emissions which are through the collision of electrons (neon lamps) and gas moreover, in order to generate the specific colors of inks, paints, and dyes the chemical compounds are used to maintain spectral characteristics.

The study is the base of the quantum mechanics development and the ground for Max Planck’s “blackbody radiation”, and the explanation of “photoelectric effect” of Albert Einstein, and the explanation of “atomic structure and spectra” of Niels Bohr. Since the atoms and molecules contain the unique spectra, thus, spectroscopy has been used in the physics and analytical chemistry. Furthermore, astronomy, telescopes, remote sensing on earth also use spectroscopy.

2.2. ELECTROMAGNETIC RADIATION

Electromagnetic radiation, in physics, refers to the “waves of their quanta and photons” in an electromagnetic field, and propagates over space which carries the electromagnetic radiant energy including radio waves, gamma rays, microwaves, infrared, visible light, ultraviolet, and X-ray (Kerker, 2016). Therefore, the molecular spectroscopy is interested in absorption or emission with electromagnetic waves and molecules which can be used to identify compounds in present and to determine molecular properties. Electromagnetic radiation demonstrates waves and particle’s properties that are known as “wave-particle duality”.

Electromagnetic radiation entails alteration of electric and magnetic fields and it has a classical description of continuous sinusoidally wave like. The figure 2.1 given below depicts the radiation of a photon which travels along the x-axis, and the electromagnetic spectrum extent showing low energy radio TV to a high energy γ radiation. There is no implied fundamental difference between the divisions of several different regions, but it indicates that there is the use of different experimental techniques.

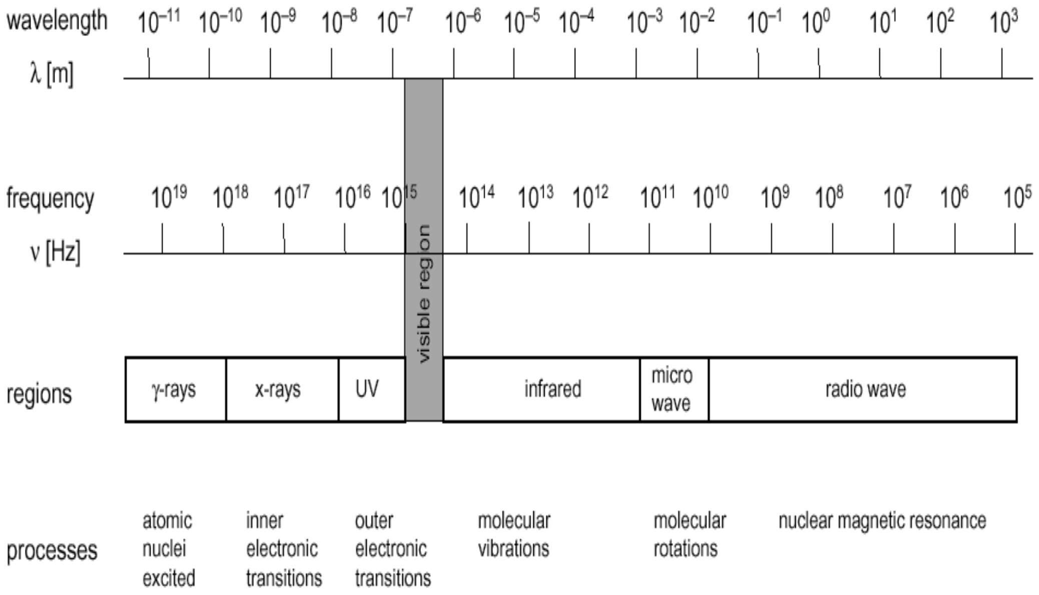
wavelength
λ [m]
10^{-11} 10^{-10} 10^{-9} 10^{-8} 10^{-7} 10^{-6} 10^{-5} 10^{-4} 10^{-3} 10^{-2} 10^{-1} 10^{0} 10^{1} 10^{2} 10^{3}
frequency
ν [Hz]
10^{19} 10^{18} 10^{17} 10^{16} 10^{15} 10^{14} 10^{13} 10^{12} 10^{11} 10^{10} 10^{9} 10^{8} 10^{7} 10^{6} 10^{5}
visible region
regions
γ-rays
x-rays
UV
infrared
micro wave
radio wave
processes
atomic nuclei excited
inner electronic transitions
outer electronic transitions
molecular vibrations
molecular rotations
nuclear magnetic resonance

Figure 2.1: Electromagnetic spectrum.

- E denotes to the electric field component radiation
- H refers to the magnetic field component and
- Vectors E and H are respectively y and z
- Thus, x-direction is the route towards which the oscillation of both electric and magnetic fields travel a velocity c, the route of propagation

$$E = E_0 \sin(2\pi \nu t - kx) \tag{2.1}$$

Accordingly, the electric and magnetic fields sinusoidally oscillate containing the frequency of $2\pi v$, and for each component k is the same. All the electromagnetic radiation travels at the same promptness in a vacuum, c (light's speed), and wavelength may characterize it in air or vacuum or with $\bar{v}$ (wavenumber) and v (frequency) where both conventionally in a vacuum.

$$\lambda = \frac{c}{v} = \frac{1}{v} \tag{2.2}$$

2.3. INFRARED SPECTROSCOPY

Infrared spectroscopy basically deals with the spectrum of electromagnetic regions that describe the light have a long wave-length and lesser rate compared to visible light. Moreover, the infrared spectroscopy is related to the ultraviolet light with a particle that is based on absorption spectroscopy.

Small portion of the electromagetic spectrum is visible to huma eye. Ultraviolet lies on the visible spectrum of immediate high energy side and Infrared, on the other hand lies on the lower energy side.

It is important to note that the particular portion of infrared region that is the most useful for organic compound analysis not immediately adjacent to the visible spectrum infact, it has a wavelength which ranges from 2,500 to 16,000 nm, along a corresponding $1.9\text{x}10^{13}$ to $1.2\text{x}10^{14}$ Hz frequency range (Scholkmann et al., 2014). For example, Figure 2.2 graphically depicts:

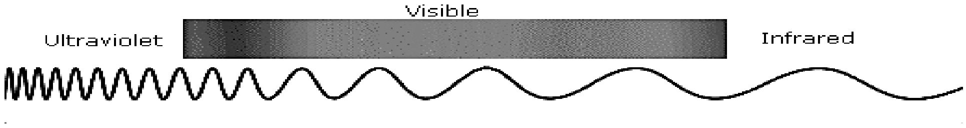

Figure 2.2: Infrared region.

2.3.1. The Vibrational Energy Of Diatomic Molecule

The diatomic molecule is only composed of two atoms which could be of same or different chemical elements. It is important to note that if two atoms of the same element are considered then it would be homo-nuclear e.g., oxygen (O_2), and if two atoms of a diatomic molecule are of different atoms then the molecule would be called hetero-nuclear e.g., nitric oxide (NO) (Le

Roy, 2017). The energy of the whole system would be at minimum when two atoms settled at a mean inter-nuclear distance and the forces of attractive and repulsive nature are balanced. Further, the repulsive forces usually rapidly rise when the atoms are very close to each other and try to pull them further apart, consequently, the attractive forces resist.

The classical mechanics enables the basis from a simple model that provides insights into the molecule vibrations. These molecular vibrations are responsible for characterizing the band scan to be observed in the given vibrational spectrum. The equation 3.1 given below demonstrates a diatomic molecule containing couple of masses of M_1 & M_2 in which a mass less spring connects (Le Roy, 2017). A diatomic molecule with a classical vibration frequency equation 2.1 stated as k which refers to the "force constant", M_1 and M_2 refers to the "masses", and μ refers to "reduced mass":

$$\bar{V} = \frac{1}{2\pi c}\sqrt{\frac{k}{\mu}} \tag{2.3}$$

In figure 3.2, k is "spring constant", M_1 and M_2 are "masses", and X_1 and X_2 refers to displaced vector of masses from symmetry with the assumption that oscillator is harmonic (Lokhov&Titov, 2016).

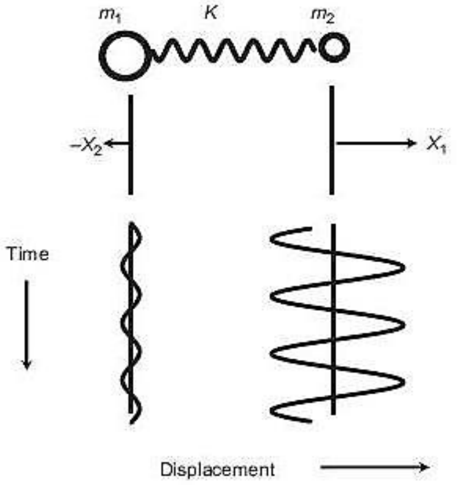

Figure 2.3: Diatomic molecule.

Schrödinger equation can be used in the calculation of vibration energy for a particular system.

$$Ev = \left(v + \frac{1}{2}\right) h\omega \tag{2.4}$$

$$\Delta v = \pm 1 \tag{2.5}$$

Δν is selection rule for harmonic oscillator.

It is pertinent to mention here that anharmonicity is a more realistic approach, though, above equation details only a harmonic oscillator is used. Furthermore, it is important to note that the dipole moment change, if does not remain linearly proportional to the nuclear displacement coordinate, then it will result in anharmoncity (Carbó-Dorca, 2016). Therefore, Figure 2.4 depicts the diagram of possible energy levels for a harmonic oscillator and anharmonic oscillator.

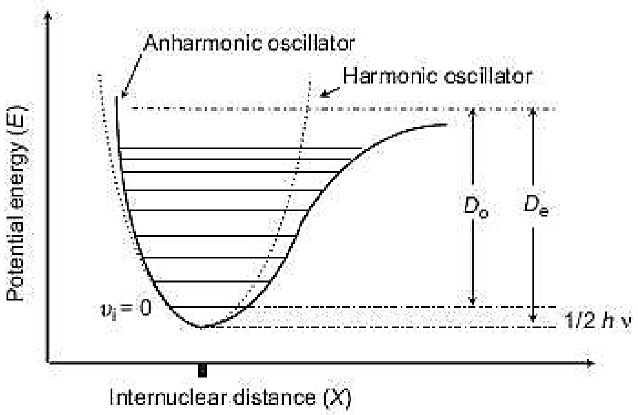

Figure 2.4: Harmonic oscillator and anharmonic oscillator.

Transitions originate from the v = 0 level and D_0 is the energy necessary to break the bond.

$$\varepsilon = \left(v + \frac{1}{2}\right)\bar{w} - \left(v + \frac{1}{2}\right)^2 \bar{w}\lambda\mathrm{e} \tag{2.6}$$

In above given equation 2.6, $\bar{w}$ is “oscillation frequency”, and χ_e is “corresponding anharmonicity constant”.

The selection rules for the anhormonic oscillator are as follows:

$$\Delta v = \pm 1, \pm 2, \pm 3 \ldots \tag{2.7}$$

2.3.2. Fundamental Vibrations

When there are three coordinates of the position of atoms (x, y, z Cartesian), thus, if a molecule has N atoms, the total number of coordinate values is 3N (Larkin, 2017):

Non- linear: 3N - 6 fundamental vibrations

Linear: 3N – 5 fundamental vibrations

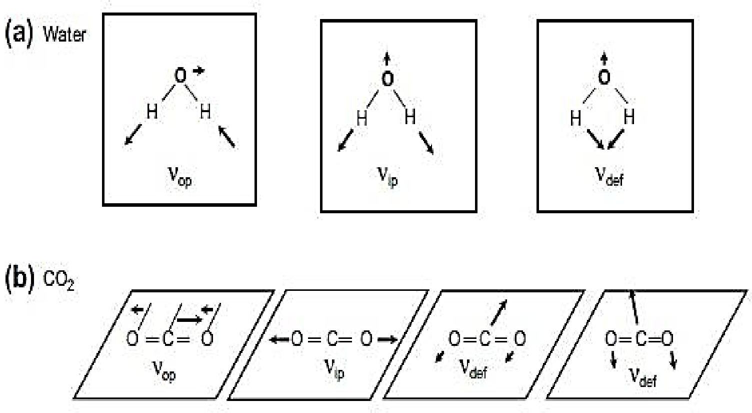

Figure 2.5: Molecular motions.

2.3.3. IR Absorption Process

The plot of intensity (absorbance or transmittance) against wavenumber poses the IR spectrum that is proportional to the ground and excited vibrational states of energy difference. The IR absorption process consists of two main components that are frequency of the radiation and dipole moment of the molecule. The resonance condition is a situation where is an interaction of the radiation and molecules in which the frequency of radiation of a specific oscillate matches with the natural frequency of a specific vibrational mode. For the transfer of energy via absorption through IR photon to the molecule, there must be a molecular dipole moment change. For IR spectroscopy, this is the acquainted rule for vibration to be IR active and it requires a consequent change in the dipole moment (Larsen, 2016).

2.3.4. IR Regions

The source obtained from a filament, and an electric current maintain the red and white heat through the most common sources the Nernst and Globar filaments. Electromagnetic spectrum in the IR spectral region takes extension from the noticeable spectrum’s red end to region of microwave that comprise of radiation consisting of wavenumbers expanded over 14,000 to 20 cm^{-1}. However, the IR region can be divided into NIR, Mid-IR (MIR) and FIR regions (Wu et al., 2014).

- The near IR region ranges from observable area at 14,000 cm^{-1} to the MIR area at 4,000 cm^{-1}
- UV-Visible spectrometersis often combined with NIR instrument
- Spectra generated in NIR region that contains several overtones and vibration modes of Mid-IR region
- “Single band spectroscopy” and “qualitative band assignments” are almost impossible because all organic species absorb in the NIR region and produce many overlapping bands

For the use of chemical analysis, the spectral range is the most useful in the MIR region which ranges from the frequency of 4000 to 500 cm^{-1}. The MIR region, furthermore, can be subdivided into group frequency region ranging from 4000^{-1} to 300 cm^{-1} fingerprint region from 1300 to 500 cm^{-1} (Shastri, 2017). It is also vital to mention here, for characterizing the molecular structure, the presence and absence of group frequency bands are very useful. Furthermore, in the fingerprint region of the spectrum, the absorption bands are the outcome of single bond and skeletal vibrations of polyatomic systems.

Finally, the FIR region ranges 500 to 20 cm^{-1} therefore, FIR region contains the lowest frequency bending and torsional motions e.g., lattice vibrations in crystals. However, the detection of the molecular vibrations is difficult to perform in the MIR region because these are very sensitive to the overall structural changes of the molecule. Though, the FIR region is the most useful for the detection and differentiation of several minerals and colorants (Wu et al., 2016).

2.4. FOURIER TRANSFORM IR SPECTROMETER

FTIR is often used as a method to acquire infrared spectra using an interferometer that collect an interferogram of a sample of solid, liquid, or gas. After collection of the interferogram, then the Fourier Transform (FT) is performed to obtain the spectrum. Therefore, the Fourier Transform IR (FTIR) Spectrometer is a process to collect and digitize the interferogram, perform the FT function, and finally display the spectrum (Baker, 2014).

The use of FTIR Spectrometer is the most suitable in infrared, spectral resolution, weak signals, quickly acquisition of spectra through extraordinary S/N ratio, and extraordinary exactness of spectrum. There are robust theoretic details behind FTIRs which allow them to shine in the above given groups. However, the maximum potential advantage depends on the design of the particular instrument and the measurement.

Furthermore, it is pertinent to mention that the “absorption spectroscopy” is used to measure the capacity of each sample to absorb light at every wave-length. Dispersive spectroscopy is a simple technique to perform do this, in which a sample of single colour beam light and absorbed light measurement, and repetition of wavelengths. On the other hand, Fourier transform spectroscopy is a more spontaneous method to collect the same kind of information compared to the single colour beam light at a given sample. This process is mostly repetitive over a time span, and finally a computer program gathers all data and helps us to conclude the absorption at each wavelength (Yang et al., 2015).

Historically, the FTIR was initiated in 1980s with the invention of interferometer that is later known as *Michelson interferometer* (detailed discussion is provided in the next section) the interferometer helped to conduct the famous experiment of determining the speed of light. It is interesting to mention here that Michelson later received a Nobel Prize on his invention in 1907 upon the efforts to exactly measure the speed of light. Interestingly, the lack of the computers at that time of Michelson has limited his work, although, he was successful in resolving several doublet spectrum problems. The unavailability of the sensitive detectors and absence of FT algorithms posed challenges for Michelson to apply his interferometer to practical problems.

Traditionally, there existed some problems in the computation of Fourier transforms of interferometer and scientists were retrained to directly invert. Instead, the guess of the spectrum was a common method to compute the inverse Fourier transforms, and then the comparison with the measured interferogram. At the third stage, the modifications were expected to make a better agreement between the guessed spectrum and the data it was a continuous process until the sufficient agreement.

Fourier transform spectroscopy came into practical existence in 1940s when interferometers were being used to measure the light, it was that time when the first Fourier transform spectrum was invented, although, the calculations of Fourier transform became possible but it remained a difficult and lengthy task. Moreover, the invention of different types of interferometer beside Michelson’s started to popup, for instance, Fabry-Perot interferometer and lamellar grating. The commercial Fourier transform spectrometers became accessible by the year 1970 that gave a significant push to the technique. Initially, the cost of the FTIR spectrometers was very high and the availability was only limited to a few famous laboratories. However, with the technological boom in upcoming years helped to reduce the costs and gave a wide accessibility of the FTIR spectrometers. Today, the use of Fourier transform spectrometers becomes widely common and computers make it possible to make analysis in seconds.

FTIR spectroscopy with the help of dedicated computer and the utilization of the interferometer forms two necessary segments of the spectroscopy. The computers give advantage to acquire the digital infrared spectral information but the most attractive advantage is to get the information through interferometer compared to the traditional ways of spectrometers (granting or prism). The control of optical components with the help of a computer, collection of data, storing data, and performing the calculations on data and resultantly producing a spectrum is possible. It is now possible to manipulate spectrum arithmetically with the direct interface from a computer to the spectrometer. FTIR spectrometer’s principle is as follows :Interferometer generates an interferogram using a signal it is a record of intensity of a signal using the infrared detector which represents it as a function of the variance in the path for couple of interferometer beams. Fourier transform of interferogram provides the spectrum and the intensity that previously refers to a function of differences in path x is subject to alteration that in result provide a spectrum s which is dependent on the frequency v. Therefore,

$$S(v) = \int_{-\infty}^{+\infty} I(x) e^{+i2\pi vx}\, dx = F^{1}[I(x)] \tag{2.7}$$

In which,

$$I(x) = \int_{-\infty}^{+\infty} S(V) e^{-i2\pi v x}\, dv = F[S(v)] \qquad (2.8)$$

In above given equations, the first integral refers to the inverse Fourier transform and the second one refers to as Fourier transform. Therefore, the first equation that provides the integral converts the interferogram I(x), that is the function of differences in the path x to spectra S (v), which is a function of frequency v. It is pertinent to mention here that the calculations were performed using a computer.

2.4.1. Basic Integral Equation

The definition of Fourier integral theorem and the principle of wave superposition provide the FTIR spectroscopy basic integral equation. Michelson interferometer's basic equation can be derived as:

Let the amplitude of wave(traveling in the z direction) incident on the beam splitter be given as

$$E(z, v)dv = E_0(v) e^{i(\bar{\omega} - 2\pi v)} dv \qquad (2.9)$$

$E_0(v)$refers to the extreme amplitude of the beam at z=0. The beam splitter divides the beam to make two separate beams. The recombination of the beams let the z1 and z2 be the travelled distance and each beam represent one reflection and the transmission of the each beam. If the coefficients of the reflection and transmission is r an t respectively, then

$$E_R(z_1, z_2, v)dv = rtE_0(v) e^{i(\bar{\omega}t - 2\pi v z)} + e^{i(\bar{\omega}t - 2\pi v z)} dv \qquad (2.10)$$

$$I(z_1, z_2, v)dv = E_R(z_1, z_2, v) E_R(z_1, z_2, v) dv \qquad (2.11)$$

$$I_R(x) = 2|rt|^2 \int_0^\infty E_0^2(v) dv + 2|rt|^2 \int_0^\infty E_0^2(v) \cos(2\pi x v) dv \qquad (2.12)$$

$$E_0^2(v) = \left(\frac{1}{\pi |rt|^2}\right) \int_0^\infty \left[I_R(x) - \frac{1}{2} I_R(0)\right] \cos(2\pi v x) dx \qquad (2.13)$$

$$S(v) \alpha E_0^2(v) = constant \int_0^\infty \left[I_R(x) - \frac{1}{2} I_R(0)\right] \cos(2\pi v x) dx \qquad (2.14)$$

2.4.2. The Michelson Interferometer

The Michelson Interferometer typically provides the base to an FTIR, and is shown in the Figure 2.6 below. As the Figure 2.6 precisely entails of a splitting beam, a fixed mirror and a translation mirror of backing and onward. Moreover, special material ray splitter is used to transmit radiation in half and striking it to resultantly reflect the other half.

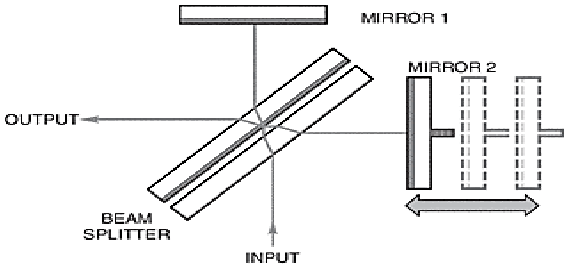

Figure 2.6: Michelson interferometer.

The Figure 2.6 also depicts two separated beams in consequence of a radiation that strikes the beam splitter thus, one beam splitter transmits the ray through fix glass and the second ray splitter transmits the ray to the moving glass. On the other hand, the radiation of two mirrors is fixed and moving reflects back to the beam splitter (Zhou et al., 2015). All over again, the radiation is transmitted and the other half of the radiation reflect the ray splitter that consequences in single ray passing through detector whereas the other half reflected spinal to the foundation.

There are three different regions in the infrared namely near infrared region, mid infrared region, and far infrared region and the boundaries between these regions vary because there is not any defined limits. The use of detector technology that gathers the light actually determines the wavelength region across three different regions. Near infrared is determined from the ground viewpoints from 1960s and it is done in the similar way of visible light observations for wavelengths and ranges from the 1 micron, however, it requires a special infrared detector to observe beyond 1 micron. On the other hand, mid infrared and far infrared region observation can be obtained from the above the atmosphere and to collect these observation there is a special detector required that contains the crystal i.e. germanium because of its heat sensitivity to the electric resistance.

The radiation heat (temperature) of any object emits the infrared radiation; therefore, every celestial object emits some infrared. The intensity of the object radiation on wavelength directly depends on the respective temperature and as the temperature decreases, and generally it is more prominent to beyond infrared wavelengths. Thus, some wavelengths infrared better suits to study in certain objects compared to the others. As we move towards the mid and far infrared regions of the spectrum, some of the celestial objects will vanish.

The C-H, N-H or O-H stretch help to make the bands and it is important to mention that the intensity of the band will be less in the bands that fall near infrared region and close to the infrared. Moreover the intensity trend is reducing with a factor of 10.

2.4.3. Attenuated Total Reflectance (ATR)

ATR is a sampling method that has been widely used in the recent times; it is one of the most used sampling tools for Fourier Transform IR (FTIR). ATR has revolutionized infrared analyses of the solid and liquid samples because it contests the preparation of the sample and the reproducibility of spectral (Jaiswal et al., 2015). Further, the ATR sampling tool helps to generate quantitative and qualitative analyses of examples through or without example planning. Comparatively, the traditional FTIR transmission sampling contains the diluted sample along through transparent salt of IR, pressed in thin film or pallet, and preventing the total absorption of bands in the “infrared spectrum”.

IR spectroscopy has several strengths but one of the superiority is the capability to obtain and analyze the spectrum from several solid, liquids and gases. It is pertinent to note that there are some samples needed to be prepared in order to acquire good quality spectrum. Conventionally, the IR spectrometers were used to directly transmit the infrared radiation from the sample to obtain analysis in that context, the intensity of the features of the spectrum were determined through the thickness of the solid or liquid sample and the thickness of the sample would not be more than a few tens of microns. However, Attenuated Total Reflectance technique made it possible to revolutionize the analyses of the solid and liquid samples in the recent years and helped to counter the several challenges of the infrared analyses by addressing the problems of sample preparation and spectrum reproducibility.

The traditional sample preparation for transmission contains few issues but a couple of the most common issues in the context of sample preparation are grinding the solid material into powder and spreading that sample on the matrix. The spread of the sample can be conducted in the liquid form as the most common way of doing that is to use the mineral oil. Classically, less than twenty milligrams of the solid and a few drops of the nujol were enough to create a paste of the sample which is spread over the matrix for spectrometer analysis using transmission.

On the other hand, the sample preparation for liquids is easily compared to the solid sample for transmission study. However, there is reproducibility issues associated with the both type of sample preparation Furthermore, the sample preparation is the most difficult and complex part of the analysis and even after the correct preparation of the sample, there exists difficulties to get the correct ratios of the sample to the matrix. Therefore, the ATR technique helps to address these issues of sample preparation and respective correct analyses.

The principles of the ATR technique suggest that it measures the changes when beam interacts with a sample and internally reflects the infrared beam. An optical dense crystal is being exposed to the infrared beam with extraordinary index of refractive with a particular angle and it internally creates an evanescent wave that reaches to the sample through the crystal surface. The evanescent wave only project few microns i.e. $0.5\mu - 5\mu$ and as a result, a decent contact is a must between the sample and the surface of the crystal. The infrared spectrum regions where the energy is absorbed, the evanescent wave will be attenuated and it will pass back the energy to IR beam that exists on the other end of the crystal and passes it to the detector in the IR spectrometer. Therefore, an infrared spectrum is generated.

In order to be successful, there are two main requirements to be fulfilled by ATR technique. First one is the direct contact between a sample and the ATR crystal because of the reason that evanescent wave only projects a few microns i.e.$0.5\mu - 5\mu$The second requirement is the significant greater value for the refractive index compare to the sample because without this condition there will not be any occurrence of the internal reflectance. If this condition is not fulfilled the light would only pass through, instead of the internal reflection in the crystal.

ATR sampling technique is a very useful tool to acquire the best quality data in combination with the good reproducibility of infrared sampling. The ATR technique has several advantages that are as follows:

- ATR technique accelerates the sampling process
- ATR technique has the ability to improve the reproducibility of the sample
- It helps to reduce the spectral variation between different users
- It helps to improve acquiring and reproduce the spectra
- It helps to build quality databases, exact confirmation, and identification
- It is one of the best technique to conduct quantitative analysis that involves liquids

2.4.4. ATR Mechanism

The ATR mechanism is a tool that guides the IR ray to a high refractive index through a crystal. Consequently, internal surface of the crystal reflects IR beam, and creates and projects orthogonally an “evanescent wave” (Ewing et al., 2015). Thus, ATR crystal creates contact with a particular sample. Therefore, the sample absorbs some fleeting wave energy, and subsequently reflects radiation which is directed back to the detector. The ATR mechanism is shown in Figure 2.7.

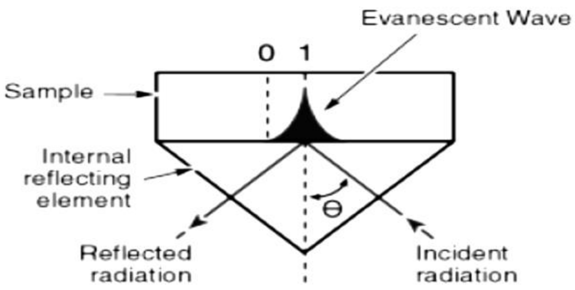

Figure 2.7: ATR Single reflection.

It is important to note that the analysis of ATR samples are relaxed but it is pertinent to note their experimental factors and their effects on the final spectrum:

- ATR crystal, the sample, and their refractive indices
- IR beam and angles of incidences
- Critical angel
- Penetration depth
- IR beam wavelength
- Effective path length and etc.

To conclude, ATR sampling tool is the most famous FTIR sampling tool because it is easy to use and enhances the quality and speed of the analysis. Moreover, ATR sampling tool makes analysis with or without sample preparation and in short time.

2.5. HARTREE FOCK APPROACH

The method of Hartree-Fock has origins back to the end of 1920s, however, D.R. Hartree introduced a method soon after the “Schrondinger equation” in 1926 the Harteree Rock approach that helps to estimate the functions of waves and the respect energy for atom and the ions.

Hartree-Fock (HF) method suggests that the N-body of functions of the system can be approximated through single Slater determinant or the single enduring of N spine orbitals. Therefore, the application of variational method helps to derive the N spine orbitals and their respective N coupled equations (Umar, Oberacker, &Simenel, 2015). Moreover, the solutions of the N coupled equations produce the Hartree Fock wave functions and the system’s energy. It is interesting to note that self-consistency and assumption of initial field are necessary conditions for distribution computing.

The Hartree Fock method is based on the earlier literature in the old quantum theory of Neil Bohr, and other researches that attempted to produce and introduce the empirical parameters in hope to achieve better experimental data. Hartree used the fundamental physical principles to explain themultiple bodies Schrodinger equation that is time independent. Thus, Hartree proposed the solutions which became Hartree Method.

2.5.1. Born–Oppenheimer Approach

Born Oppenheimer approach is a method which belongs or belonging) to molecular physics that assumes the motion of atomic nuclei and the associated electrons can be detached. BO method consists of two names “Born” and “Oppenheimer” that is associated with the names of the scientists. Moreover, the Born Oppenheime restimation can be described in mathematical expressions that broke the molecule wave functions into vibrational or rotational nuclear and electronic components.

$$\Psi_{total} = \lambda_{electronic} \times \lambda_{nuclear\ independent} \qquad (2.15)$$

$$\Psi_{total} = \Psi_{el}\Psi_{vib}\Psi_{rot}(motions\ are\ independent) \tag{2.16}$$

$$E_{tot} = E_{el} + E_{vib} + E_{rot}(E_{el} \gg E_{vib} \gg E_{rot}) \tag{2.17}$$

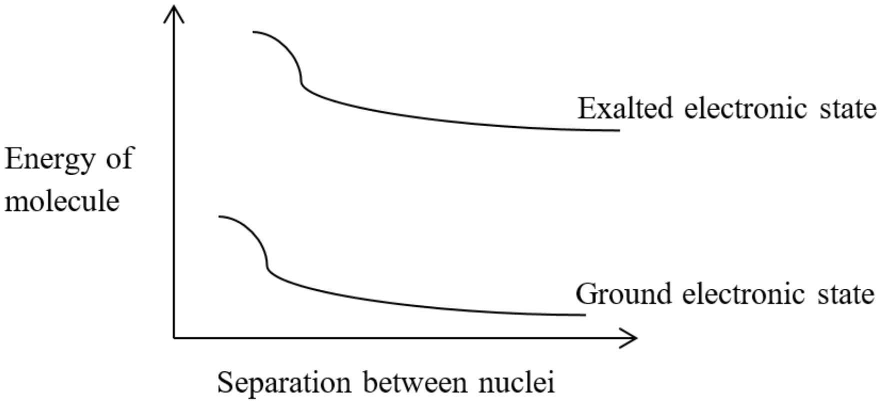

Figure 2.8: Potential energy curves.

The approximation of the computational energy and wave-function of a molecule (average-size) help to simplify, for instance, there are twelve nuclei and forty two electrons in “benzene molecule” (Braaten, Langmack, & Smith, 2014). For Born-Oppenheimer approximation, the first step is to solve the “electronic Schrondinger equation” that solution produces the χ electronic wave-function that depends on the electrons only. As far as the benzene, there are 126 electronic coordinates in benzene wave-function.

Furthermore, nuclei are fixed in a particular formation though these are often resulted in an equilibrium formation during the approximation process. For instance, the electronic computation has to be in nuclear coordinates because there is a vibrational spectrum required in the study of nuclear motion in quantum mechanics and its effects. Second step in the process of Born-Oppenheimer approximation is the containment of nuclei only in the Schrondinger equation and there are 36 variables in the equation of benzene (Braaten, Langmack, & Smith, 2014).

Born Oppenheimer approximation is related to the separate components of energy in the context of molecular spectroscopy. Moreover, everal ratios including electronic periods, vibration energy, and rotation energy has relation with the scales.

$$E_{total} = E_{electronic} + E_{vibrational} + E_{rotational} + E_{nuclear} \tag{2.18}$$

2.5.2. AB Initio Method

Ab initio method, in nuclear physics, seeks to "describe the atomic nucleus form the ground up by solving the non-relativistic Schrodinger equation for all constituent nucleons and the forces between them" (Chinesta&Abisset-Chavanne, 2018). In comparison to the other methods such as "nuclear shell model", the ab initio method is a more fundamental approach. It is important to mention here that ab initio method was only applicable to very light nuclei, however, the recent progress in terms of evolution of the ab initio method has made it useful for heavy nuclei e.g. Nickel.

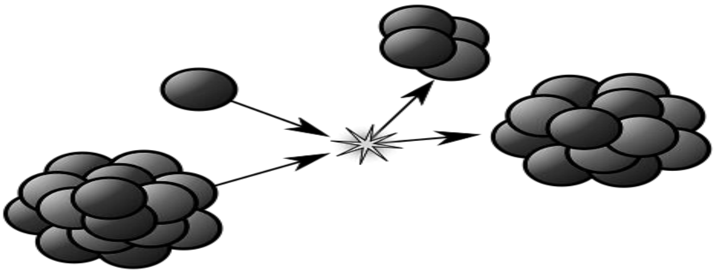

Figure 2.9: Nuclear reaction.

The inter-nucleon interaction and the complexities of these interactions when attempted to give a treatment using ab initio is a significant challenge for this method. The "quantum chromo-dynamics" describes the strong nuclear force that is usually emerged from the strong interaction which is resulted from "quantum chromo-dynamics (QCD)" however; QCD is relevant to nuclear physics which is a"non-pertubative in the low-energy regime".

2.6. DENSITY FUNCTIONAL THEORY

In physics and chemistry, it is computational quantum mechanics model that helps to examine the structures of electronic of several systems which are usually in the ground state. Particularly, it is used to investigate the atom, molecule, and the compressed phase. The density functional theory helps to determine the properties of many electron systems therefore, in the case of functionals, it is spatial reliant on density of electron .Thus, the use of functional of the electron density has been derived from the model.

Until 1970s, the calculation of solid state physics remained the most popular for the density functional theory, though, the calculations of quantum chemistry until 1990s proved inaccurate measure. However, the density functional theory has been revised and evolved to a better model that is now able to measure the “exchange and correlation interactions”. Furthermore, the density functional theory is very useful in terms of the computational costs comparing the traditional method.

It is pertinent to mention here that despite the recent developments in the theory and its usefulness to computational physics the theory still finds itself in a difficult position when it comes to describe “intermolecular interactions that is critically important to understand the chemical reactions”, especially, the use of the theory is difficult in van der Waals, excitement of transfer charge, transitional states, global potential energy, interactions of do pant, and other strong correlation systems (Bechstedt, 2015).Furthermore, the application of theory is also difficult in the estimation of band gap and semiconductor’s ferromagnetism.

The accuracy of the density functional theory is adversely affected when the treatment of dispersion is concerned, not for all, but particularly in a system’s treatment that is being dominated by dispersion and the significant effects of biomolecules. There are three types that are used in density functional methods, which are as follows (Bechstedt, 2015):

- The approximation of local density: this type of method is based on the assumption that molecule density is uniform all over the molecule and it is not considered a valuable method
- The methods of gradient-corrected: these methods measure the electron density for their non-uniformity
- The hybrid methods: As the name suggests, it combines several features of ab initio methods and some aspects of the DFT mathematics. The most common used hybrid methods in computational chemistry are B3LYP.

As it has been previously described in with some detail that density functional theory is applicable to most of the systems as a computational method, and it is useful for some type of calculations than others.

2.6.1. Basis Sets

As we proceed to the density functional theory to basis sets that make it possible to use the electronic wave function in Hartree Fock method that produces algebraic equations from partial differential equations for implementation efficiency on a computer.

The approximation of resolution of the identity is equivalent to the use of the basis sets, the basis-functions of linear combinations are being expressed by the single particle states of molecular orbitals. The atomic orbitals that yield linearity mixture of atomic orbitals can be originated on the basis sets and has been widely popular in quantum chemistry scholars, on the other hand the solid state community uses the plane waves (Roos et al., 2016).For instance, Gaussian, Slater, and numerical type orbitals represent several types of the atomic orbitals.

Among the given examples of all three types of atomic orbitals, Gaussian type orbitals are the most commonly used because it allows “Post-Hartree-Fock methods” to be implement efficiently. Moreover, wave functions are being represented by a vector along with a basis setand coefficients of basis-functions which correspond in the linear expansion within the components of the wave-function.

2.6.2. Gaussian Program

Gaussian is a software program developed in Carnegie Mellon University in 1970 and was initially released during the same year with the name Gaussian 70. John Pople and his other research fellows developed this software program for the computational chemistry. Since then, the software has been widely adopted, though; the name of the software has been derived from the use of “Gaussian orbitals” that had been used to speed up the calculations of molecular electronic structure as compared to the use of “Slater type orbitals” (Richings et al., 2015). The use of “Gaussian orbitals” instead of “Slater type orbitals” was adopted to improve the performance of the limited capacity of the computing facilities at that time, and the earlier use of “computer hardware for Hartree-Fock calculations”.

2.7. GEOMETRY OPTIMIZATION

Geometry optimization which also refers to optimization of energy, minimization of geometry or energy minimization is a process that finds an arrangement in space for the collection of atoms. According to some computational models of chemical bonds the total interatomic force of every atom is at the accepted range which is close to zero and there is stationary point on the potential energy surface. Furthermore, the selection of the molecule, ion, condensed phase, or a transition state can be a single one or it could be the aggregation of these. For instance, chemical bonding of computation model might be a quantum mechanics (Birkholz& Schlegel, 2016).

For example, the optimization the geometry of the water molecule generates the desired outcome in the form of bond lengths of hydrogen and oxygen or the bond angles of hydrogen and oxygen. Moreover, the optimization minimizes the forces which otherwise pull and push the atoms together. The values of different geometry and related single point energy displays in three dimensional graph, which is as follows:

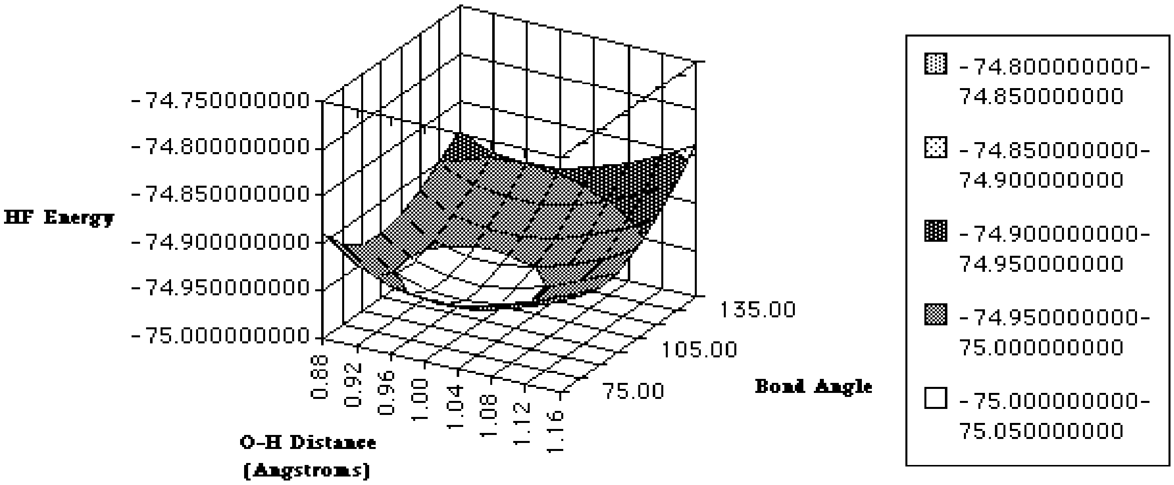

Figure 2.10: Single point Hartree-Fock energies for water molecule.

There are distinct points that show the potential energy surfaces (Birkholz& Schlegel, 2016):

- Maximum local is the highest value in the PES region or the particular section of the potential energy surface
- Maximum global is the uppermost value in the whole PES region that points of the potential energy surface
- Minima local is the lowermost value on the PES region that surfaces on the potential energy
- Minima global is lowest value in the entire PES region
- Saddle point refers to a hybrid point which at the same time represents a highest value and the lowest value on the PES. The saddle point connects tow equilibrium structures.

In order to illustrate these points graphically on graph, Figure 12.2 represents the two dimensional graph:

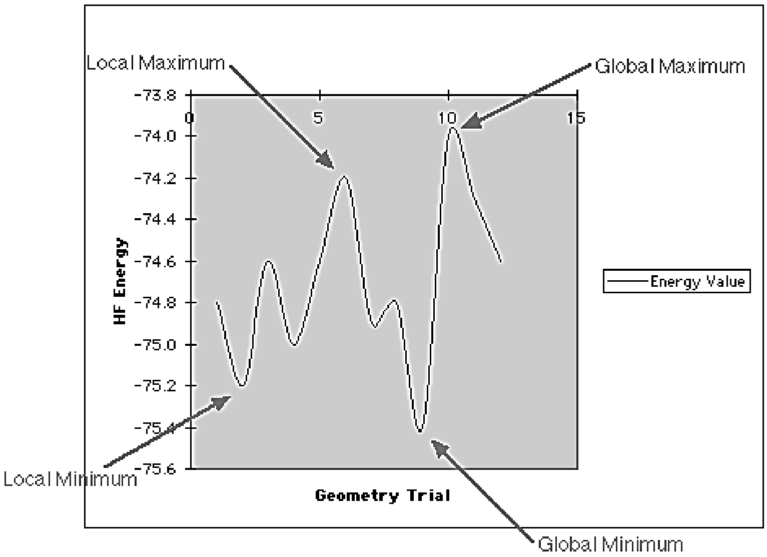

Figure 2.11: Molecular geometry vs. HF energy.

2.8. VIBRATIONAL FREQUENCIES

The vibrational frequencies are generated through the molecular vibrations on the basis of periodic motion in the atoms of a molecule whereas the rotation motion and translation of molecule remains constant. Moreover, the periodic motion and the frequency associated with it refer to the vibrational frequency and these frequencies ranges from 10^{13}-10^{14}

approximately(Sathyanarayana, 2015). Furthermore, the modes of vibration vary with the number of atoms that are:

- The modes of vibration for molecule with N atoms would be 3N-6
- The modes of vibration for a linear molecule would be 3N-5 because molecule's axis rotation cannot be observed
- The vibration for a normal mode would be one in case of a diatomic molecule
- The polyatomic molecule's normal mode of vibration would be independent of each other
- Diverse chemical bonds of each molecule will involve with each normal mode and respective vibrations

The process of molecule vibration starts when a molecule absorbs the quantum of energy that denotes to E, and that energy corresponds with the V (frequency) and h (constant) in the given equation $E = hv$.

In order to approximate the vibrational frequencies, the first approximation can be called a "simple harmonic motion" that is denoted to a normal vibration. Parabola refers to the vibration energy in the context of displaced atomic and respective frequency is twice for the first overtone (Sathyanarayana, 2015). In the context of realism, the vibrations are basically an harmonic and the fundamental frequency which is twice, is a bit lower in the case of first overtone. Therefore, in order to excite the higher overtones, there is less additional energy is required to progress and subsequently led to the "dissociation of the molecule", and the Morse potential is the main motive behind the potential energy of a molecule. Furthermore, there are several ways to probe the vibrational state of the molecule and infrared spectroscopy provide the most direct way to do this. Moreover, the Roman Spectroscopy is a distinct method that helps to directly measure the vibrational frequencies.

2.9. TRANSITION METAL COMPLEX

The transition metal complex consists of the molecules or ions that are binding to transitional metal ions which form complexes. The coordination complexes refer to a creation of Lewis acid base reactions that through covalent bond attached the natural molecules or anion to a central metal atom (Abu-Dief& Mohamed 2015).

- Ligands refer to the complex agents that contain at least one pair of electrons giving to a metal atom and Lewis base.
- Metal atoms refer to acid that absorb the electrons pairs from the bases of Lewis
- Donor atom is an atom inside a ligand the bounds directly to the metal atom
- Complex ion is net charge of coordination complex
- Coordination compound hold the coordination complex

The details of some coordination complex are as follows:

Table 2.1: Examples of coordination complex.

Example	Molecular Formula	Lewis Base	Lewis Acid	Donor Atom	Coordination Number
	$[Ag(NH_3)_2]^+$	NH_3	Ag^+	N	2
	$[Zn(CN)_4]^{2-}$	CN^-	Zn^{2+}	C	4
	$[Ni(CN)_4]^{2-}$	CN^-	Ni^{2+}	C	4
	$[PtCl_6]^{2-}$	Cl^-	Pt^{4+}	Cl	6

2.10. NORMAL COORDINATES

Q is the sign which denotes to the normal coordinates, and it refers to the atom's position in a distance from the equilibrium points that are in the context of normal mode of vibration. As the name suggests, normal coordinates hold a single coordinate and it has been assigned to a each single mode therefore, normal coordinate progress along with the normal mode at any point in time (Zimmerman &Smereka 2016).

The secular determinant solution provides the normal modes and the normal coordinates express Cartesian coordinates over summation. One of the major benefit to work with normal modes is their diagonal matrix governs the vibrations of molecule and in that process each and every normal mode behaves independently of molecular vibration. Therefore:

- If a molecule possesses symmetry elements, it will belong to the point group
- Under that group, each normal mode will transform to "an irreducible representation"
- If we apply the group theory on that normal modes, we will get qualitative data that project the complex depiction coordinates of Cartesian

For instance, if the treatment applied to CO2, we will get the following (Zimmerman &Smereka 2016):

- Symmetry Stretch is the amount of stretching coordinates C-O and the changes in the bond length will change by the same amount and the status of carbon atom will be motionless $Q = q1 + q2$

- Asymmetry Stretch refers to the difference between two coordinates C-O and there will be increase in the length of the one bond and a decrease in the other bond $Q = q1 - q2$

2.11. INTERNAL COORDINATES

The internal coordinate have six different types, illustrated i below figure:

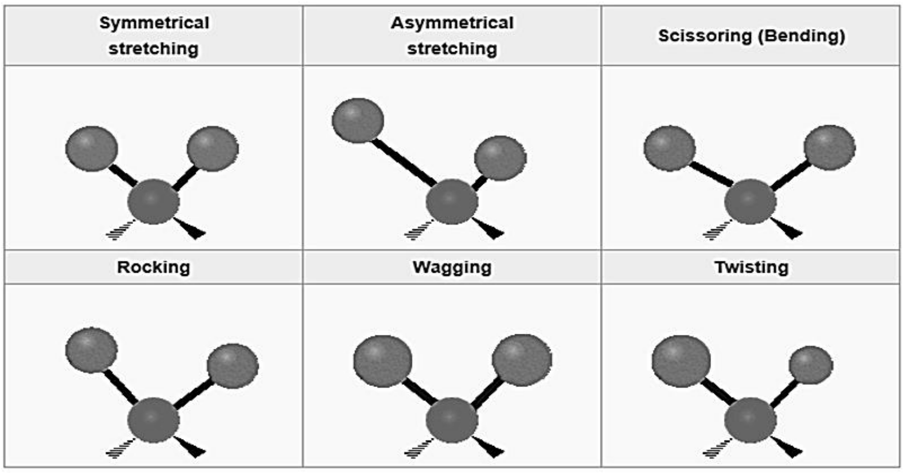
Symmetrical stretching
Asymmetrical stretching
Scissoring (Bending)
Rocking
Wagging
Twisting

Figure 2.12: Vibrations of methylene group in a molecule.

The details of these six internal coordinates are as follows in the table below:

Table 2.2: Details of six internal coordinates.

Type	Detail
Streching	Changes in the bond length e.g. C-H or C-C
Bending	Changes in the angles of two bonds
Rocking	Changes in the angles of atom group
Wagging	Changes in the angle between plane of a group atoms
Twisting	Changes in the angel between two groups of atoms and their planes

3. RESULTS

The geometry optimization and vibrational wavenumber calculations of the complex were achieved by density functional theory (DFT) using B3LYP functional with 6-31G(d,p) basis set using Gaussian. The initial structure of the prothionamide molecule was generated using previously reported geometry parameters in a previous study (Yilmaz&Bolukbasi, 2016). The optimize geometry of the complex was then calculated. The calculated wavenumbers were scaled by a factor of 0.961. The vibration modes were interpreted using potential energy distributions (PED). The GAR2PED program was used to calculate the PED values. Optimized geometry parameters of complex are given in Table 3.1 and Figure 3.1 displays the optimized geometry of the complex. Experimental wavenumbers, calculated wavenumbers, scaled wavenumbers and PED values are given in Table 3.2. The energy of the complex E(UB3LYP) which belongs to optimized geometry is found as -3418.05568350 a.u. The theoretically predicted IR spectra of the complex are given in Figure 3.2. An experimental FTIR spectrum of the complex was recorded in the range of 4000–600 cm^{-1} which is given in Figure 3.3.

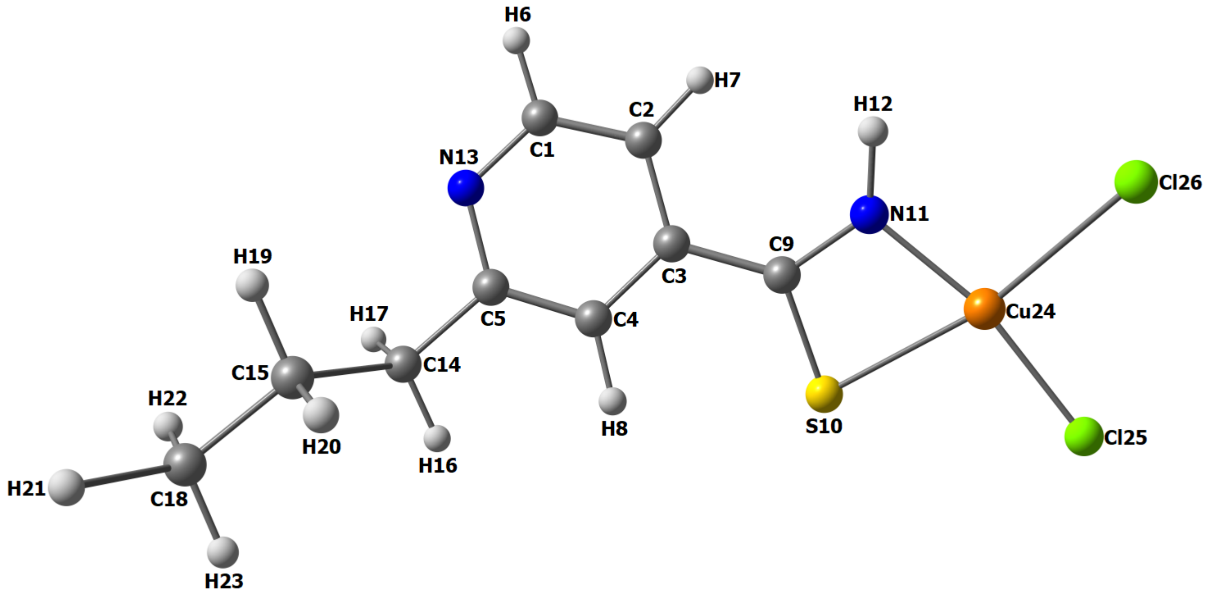

Figure 3.1: Optimized geometry of the complex.

Table 3.1: Optimized geometry of the complex.

Bond Distances(Å)

R(1-2)	1.393	R(11-12)	1.014
R(1-6)	1.088	R(11-24)	1.864
R(1-13)	1.337	R(14-15)	1.542
R(2-3)	1.401	R(14-16)	1.096
R(2-7)	1.085	R(14-17)	1.096
R(3-4)	1.399	R(15-18)	1.530
R(3-9)	1.468	R(15-19)	1.096
R(4-5)	1.401	R(15-20)	1.098
R(4-8)	1.085	R(18-21)	1.094
R(5-13)	1.345	R(18-22)	1.096
R(5-14)	1.509	R(18-23)	1.096
R(9-10)	1.752	R(24-25)	2.129
R(9-11)	1.298	R(24-26)	2.156

Table 3.2 (contiued): Optimized geometry of the complex.

R(10-24)	2.261		
Bond Angles(^{o})			
A(2-1-6)	120.0	A(9-11-24)	103.8
A(2-1-13)	123.8	A(10-24-11)	72.7
A(1-2-3)	117.9	A(10-24-25)	95.4
A(1-2-7)	120.2	A(10-24-26)	166.6
A(6-1-13)	116.2	A(12-11-24)	130.5
A(1-13-5)	118.6	A(11-24-25)	168.1
A(3-2-7)	121.8	A(11-24-26)	93.9
A(2-3-4)	118.5	A(15-14-16)	109.9
A(2-3-9)	121.2	A(15-14-17)	108.9
A(4-3-9)	120.3	A(14-15-18)	112.5
A(3-4-5)	119.4	A(14-15-19)	108.3
A(3-4-8)	120.3	A(14-15-20)	109.2

Table 3.3 (contiued): Optimized geometry of the complex.

A(3-9-10)	125.9	A(16-14-17)	107.4
A(3-9-11)	127.1	A(18-15-19)	110.2
A(5-4-8)	120.2	A(18-15-20)	109.9
A(4-5-13)	121.7	A(15-18-21)	111.1
A(4-5-14)	121.8	A(15-18-22)	111.2
A(13-5-14)	116.5	A(15-18-23)	111.4
A(5-14-15)	112.5	A(19-15-20)	106.6
A(5-14-16)	109.9	A(21-18-22)	107.7
A(5-14-17)	108.2	A(21-18-23)	107.7
A(10-9-11)	107.0	A(22-18-23)	107.6
A(9-10-24)	76.4	A(25-24-26)	98.0
A(9-11-12)	125.1		

A:Bond angle, R: Bond distance.

Table 3.4: Comparison of the experimental wavenumbers (cm^{-1}) and theoretical harmonic wavenumbers (cm^{-1}) of the complex calculated by B3LYP with 6-31G(d,p) basis set

Wavenumbers			
Calculated	Scaled by 0.961	Experimental	PED
18	16.876121		58% τCu-N-C-Cu, 40% τCu-S-C-Cu
26	24.5556642		30% τC-C-C-N, 20% τCu-C-C-C, 12%δC-C-Cu,6% τCl-Cu-C-S
35	33.7188953		43% τC-C-C-N, 20% τCl-Cu-C-S, 16% δC-C-Cu,7% τCl-Cu-S-C
65	62.1111598		15% δC-C-C, 13% δC-C-Cu, 8% δC-C-S
70	67.2474165		36% δC-Cu-Cl, 30% δS-Cu-Cl, 22%τCl-Cu-C-S ,12% δC-C-Cu
92	88.7225952		71% τC-C-C-C, 8%δN-Cu-Cl, 8% τC-C-C-N, 7% δS-Cu-Cl
104	100.35723		26% γC-(C,N,C), 20% δC-C-C, 11% τC-C-C-N,8% τN-C-C-C
134	129.0224185		28%γC-(C,C,C), 20% δS-Cu-Cl, 19% δC-Cu-Cl,15% δCl-Cu-Cl
144	137.9250264		62% δCl-Cu-Cl, 33% δN-Cu-Cl

Table 3.5 (continued): Comparison of the experimental wavenumbers (cm^{-1}) and theoretical harmonic wavenumbers (cm^{-1}) of the complex calculated by B3LYP with 6-31G(d,p) basis set

154	148.1407447	35% δS-Cu-Cl, 30% δC-Cu-Cl, 22% δN-Cu-Cl ,13% δN-Cu-Cl
202	194.3069925	42% τCl-Cu-N-C, 33% δCl-Cu-Cl, 21% τCu-C-C-C, 4% δN-Cu-Cl
209	201.2386855	29% δS-Cu-Cl, 23% δC-Cu-Cl, 14% νCu-C, 10% νC-C
248	238.2861965	96% τH-C-C-C
262	252.0939406	30% δC-C-C, 20% τN-C-C-C, 17% τC-N-C-C
284	272.5625679	31% νCu-S, 26% νCl-Cu, 7% δS-C-Cu, 3% δC-S-Cu
310	298.0545344	19% δC-C-C, 10% νC-C, 7% δC-C-S,6% δC-C-C
327	313.9638894	27% δC-C-C, 10% δN-C-C, 7% δC-C-S
380	365.0859181	55% νCl-Cu, 9% δN-C-C, 8% δC-C-C,3% νCl-Cu
398	382.0401684	65% νCl-Cu, 11% νCu-S, 5% νCl-Cu,3% δN-Cu-Cl
409	393.4052427	18% νCl-Cu, 9% δC-C-Cu, 9% τC-C-C-C,9% δC-C-C

Table 3.6 (continued): Comparison of the experimental wavenumbers (cm^{-1}) and theoretical harmonic wavenumbers (cm^{-1}) of the complex calculated by B3LYP with 6-31G(d,p) basis set

445	427.6183803		22% τC-N-C-C, 12% τC-C-C-N, 9% τC-C-C-C,6% γC-(C,C,C)
517	496.9212797		18% γC-(C,N,C), 12% τC-C-C-N, 9% τC-C-C-C,6% δS-Cu-Cl
548	526.7067059		19% δC-C-C, 8% δC-N-C, 8% δC-C-S
587	564.4181718		49% δC-N-H, 26% δH-N-Cu, 4% δC-N-Cu, 4% τCl-Cu-C-S
620	596.2848357	621	10% δC-C-N, 5% τCu-C-C-C, 5% δC-C-C,5% δC-C-C
646	620.8064805	648	26% νCu-N, 21% δH-N-Cu, 11% νS-C, 10% δC-N-Cu
689	662.5564528		18% τCu-C-C-C, 17% γC-(C,C,C), 10% γC-(C,N,C), 5% δC-C-C
724	695.3381809	718	12% δC-N-C, 7% δH-N-Cu, 7% δC-C-N,6% νC-C
754	724.4698388	727	54% δC-C-H
764	734.6089654	751	24% τC-N-C-C, 13% τN-C-C-C, 11% τC-C-C-C
848	814.52438	824	46% γH-(C,C,C), 16% γH-(C,C,N), 6% γC-(C,C,C), 4% νC-C

Table 3.7 (continued): Comparison of the experimental wavenumbers (cm^{-1}) and theoretical harmonic wavenumbers (cm^{-1}) of the complex calculated by B3LYP with 6-31G(d,p) basis set

870	835.8780883	847	24% γH-(C,C,C), 10% νC-C, 5% δC-C-H, 5% γH-(C,C,N)
884	849.093472	868	52% δC-C-H
905	870.1433121	901	41% νC-C, 13% δC-C-H, 8% γH-(C,C,C)
928	891.4724188	912	80% γH-(C,C,C), 7% γC-(C,N,C), 5% δC-C-H, 3% γC-(C,C,C)
988	949.5969662	964	75% γH-(C,C,N), 25% γH-(C,C,C)
1013	973.6018813	971	31% νC-C, 10% δC-C-C
1049	1008.3768195	1010	87% νC-C
1093	1049.9048008	1033	47% δC-C-H
1113	1069.8094172	1088	35% δC-C-H, 19% νC-C, 10% δC-C-H, 8% δC-C-C
1147	1102.0542346		37% δC-C-H, 15% νC-C
1177	1131.1493745		22% δC-N-H, 14% δH-N-Cu, 21% δC-C-H
1224	1176.4973308		19% δC-N-H, 17% δC-C-H, 8% δH-N-Cu

Table 3.8 (continued): Comparison of the experimental wavenumbers (cm^{-1}) and theoretical harmonic wavenumbers (cm^{-1}) of the complex calculated by B3LYP with 6-31G(d,p) basis set

1256	1207.1644745	1201	45% δC-C-H
1289	1238.8567169	1233	23% νC-C, 15% δC-C-H
1306	1255.3386357	1272	53% νN-C
1324	1272.1486399		55% δC-C-H
1327	1275.6555211		19% νN-C, 11% δH-C-N, 8% νC-C, 7% δC-C-H
1347	1294.0801014	1306	30% δC-C-H, 10% δH-C-N
1389	1335.2746157		50% δC-C-H
1428	1372.3592213		37% δH-C-H, 30% δC-C-H
1432	1376.5003625	1378	25% νC-C, 18% δC-C-H
1495	1437.073634	1400	79% δH-C-H, 11% δC-C-H
1509	1450.22588	1430	80% δH-C-H
1495	1437.073634	1400	79% δH-C-H, 11% δC-C-H
1509	1450.22588	1430	80% δH-C-H
1513	1454.2064381	1447	93% δH-C-H

Table 3.9 (continued): Comparison of the experimental wavenumbers (cm^{-1}) and theoretical harmonic wavenumbers (cm^{-1}) of the complex calculated by B3LYP with 6-31G(d,p) basis set

518	1458.4483882	1469	23% δC-C-H, 17% δH-C-N, 11% νN-C
1524	1464.2841568	1485	78% δH-C-H
1602	1539.6685525	1548	35% νN-C, 20% νC-C
1619	1555.645658	1604	33% νN-C, 17% νC-C
1645	1581.3018594	1622	47% νC-C, 6% νN-C
3038	2919.5898828	2878	100% νH-C
3041	2922.4378063		100% νH-C
3050	2931.0082926	2938	100% νH-C
3078	2957.8712217		100% νH-C
3097	2976.6594444	2960	100% νH-C
3114	2992.9861617		100% νH-C
3119	2997.0618588		100% νH-C
3176	3052.5773873		100% νH-C
3204	3079.4502147		100% ν H-C
3209	3083.6460368	3120	100% νH-C

Table 3.10 (continued): Comparison of the experimental wavenumbers (cm^{-1}) and theoretical harmonic wavenumbers (cm^{-1}) of the complex calculated by B3LYP with 6-31G(d,p) basis set

3591	3451.2256538	3276	99% νH-N

ν, stretching; δ, in-planebending; γ, out-of-planebending; τ, torsion.

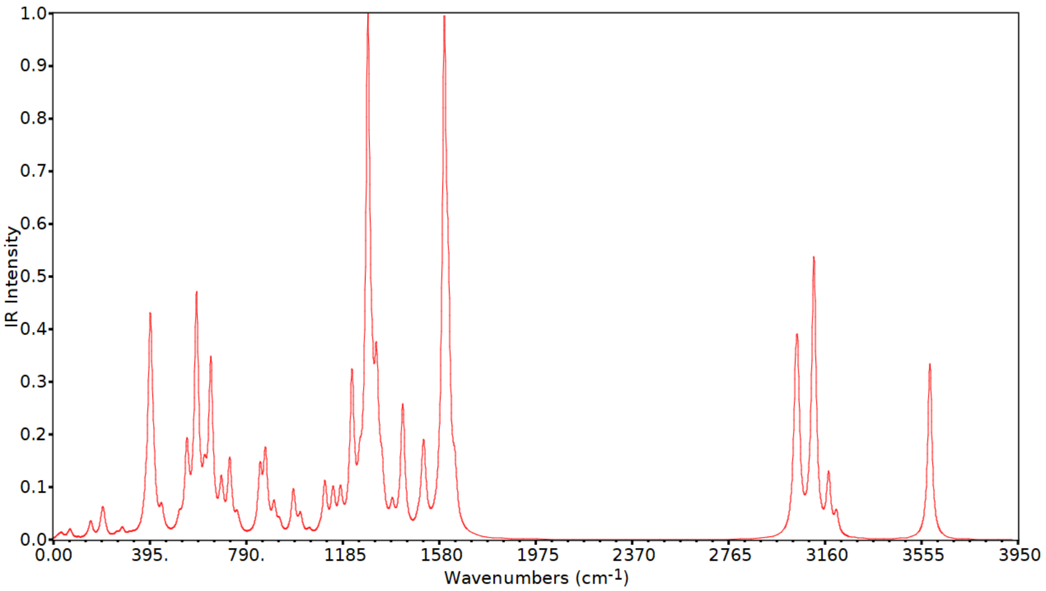

Figure 3.2: Calculated IR spectrum of the complex.

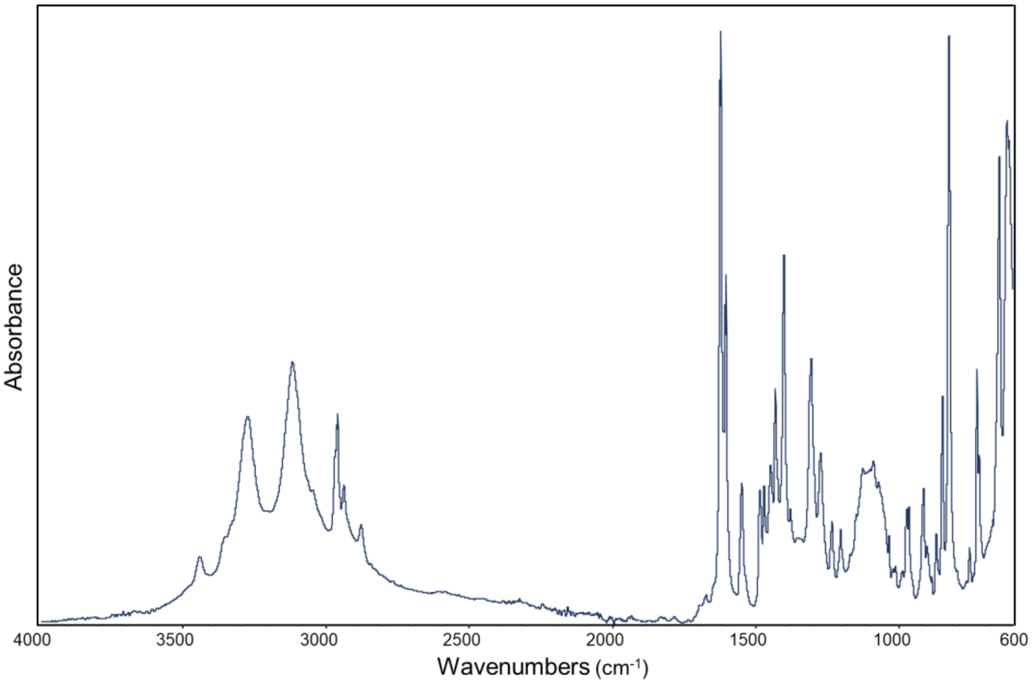

Figure 3.3: FT-IR spectrum of the complex

4. DISCUSSION

Quantum chemical calculations were performed using the Gaussian package software. The optimized geometry and vibrational wavenumbers of the copper complex of prothionamide were calculated using the DFT/B3LYP method, 6-31G ++(d, p) and basis set. The initial structure of the prothionamide molecule was generated using previously reported geomerty parameters in a previous study (Yilmaz, A., & Bolukbasi, O. 2016). The optimized geometry of the complex was then calculated.

As a result of the optimized geometry calculations, the bond lengths (C-C) and (C-N) in the ring were found to be around 1.40 Å and 1.34 Å, respectively. The bond lengths of (C-N), (C-S), (Cu-S), (Cu-N) and (Cu-Cl) were found to be about 1.30 Å, 1.75 Å, 2.26 Å, 1.86 Å and 2.13-2.15 Å, respectively. In the calculations made using DFT method, the C-C-C-S, C-C-C-N and C-N-Cu-Cl dihedral angles were found to be 19.24882, 19.09025 and -177.86934 degrees, respectively.

The vibrational modes of the prothionamide molecule were determined by considering their potential energy distributions (PED). The GAR2PED program was used to calculate potential energy distributions. The calculated wavenumbers are generally higher than the experimental values. This is due to basis set incompleteness and neglecting the vibrational anharmonicity. Therefore, the calculated wavenumbers of the B3LYP/6-31G ++ (d, p) basis set were scaled using a factor of 0.961. The calculated wavenumbers, the scaled wavenumbers, the experimental wavenumbers and the description of the normal modes based on the PED values are given in the Table 3.2. To compare the experimental and theoretical spectra, theoretical IR simulations were plotted using a Lorentz profile and a Full Width at Half Maximum (FWHM) of 5 cm^{-1}.

The bond stretching vibrations of the amide group (NH_2) are observed at about 3350-3150 cm $^{-1}$. It is seen that the PED values of the bond stretching vibrations of the amide group are quite pure. The band at 3276 cm^{-1} in the IR spectrum belongs to the bond symmetric stretching vibrations of the amide group. In the 3100-2800 cm-1 region in the spectrum, the bands can be labeled as stretching vibrations of CH, CH_2 and CH_3. The band at 1272 cm $^{-1}$ may due to CN bond stretching vibrations. The PED values of this vibration were found to be 53%. The band at 1604 cm^{-1} can be marked as ring breathing vibration mode. According to PED values, it can be said that the bond stretching vibrations of (Cu-S), (Cu-N) and (Cu-Cl) can be observed in the IR spectrum at 273, 646 and 380-400 cm $^{-1}$, respectively.

5. CONCLUSION AND RECOMMENDATIONS

As a result, optimized geometry parameters of the copper complex of prothionamide were calculated using the DFT/B3LYP method, 6-31G ++ (d, p) basis set. Vibrational modes of the coordination bonds in the complex were determined by PED. The calculated wavenumbers and the band intensities of the complex were found to be in good harmony when compared with the experimental values.

REFERENCES

Abu-Dief, A. M., Mohamed, I. M., 2015, A review on versatile applications of transition metal complexes incorporating Schiff bases. *Beni-suef university journal of basic and applied sciences*, 4(2), 119-133.

Baker, M. J., Trevisan, J., Bassan, P., Bhargava, R., Butler, H. J., Dorling, K. M., Heys, K. A., 2014, Using Fourier transform IR spectroscopy to analyze biological materials, *Nature protocols*, 9(8), 1771.

Bechstedt, F., 2015, Density Functional Theory Many-Body Approach to Electronic Excitations, *Springer*, 73-88.

Bernheim, F., Bernheim, M. L., 1931, Pyrrole As A Catalyst For Certain Biological Oxidations. *Journal of Biological Chemistry*, 92(3), 461-469.

Birkholz, A. B., Schlegel, H. B., 2016, Exploration of some refinements to geometry optimization methods. *Theoretical Chemistry Accounts*, 135(4), 84.

Braaten, E., Langmack, C., Smith, D. H., 2014, Born-Oppenheimer approximation for the X Y Z mesons. *Physical Review D*, 90(1), 014044.

Carbó-Dorca, R., 2016, About an incoherent precision behavior in LCAO MO theory when a simple diatomic molecule collapses into an atom, *Journal of Mathematical Chemistry*, 54(4), 845-848.

CCCBDB, 2018, *Precomputed vibrational scaling factors*, Retrieved 01 May, 2018, https://cccbdb.nist.gov/vibscalejust.asp

Chinesta, F., Abisset-Chavanne, E., 2018, Ab-Initio Calculations A Journey Around the Different Scales Involved in the Description of Matter and Complex Systems, *Springer*, 29 - 39.

Ewing, A. V., Biggart, G. D., Hale, C. R., Clarke, G. S., Kazarian, S. G., 2015, Comparison of pharmaceutical formulations: ATR-FTIR spectroscopic imaging to study drug-carrier interactions, *International journal of pharmaceutics*, 495(1), 112-12-121.

Fajardo, T. T., Guinto, R. S., Cellona, R. V., Abalos, R. M., Cruz, E. C. D., Gelber, R. H., 2006, A clinical trial of ethionamide and prothionamide for treatment of lepromatous leprosy, *The American journal of tropical medicine and hygiene*, 74(3), 457-461.

Frisch, M. J., Trucks, G. W., Schlegel, H. B., Scuseria, G. E., Robb, M. A., Cheeseman, J. R., Scalmani, G., Barone, V., Mennucci, B., Petersson, G. A., Nakatsuji, H., Caricato, M., Li, X., Hratchian, H. P., Izmaylov, A. F., Bloino, J., Zheng, G., Sonnenberg, J. L., Hada, M., Ehara, M., Toyota, K., Fukuda, R., Hasegawa, J., Ishida, M., Nakajima, T., Honda, Y., Kitao, O., Nakai, H., Vreven, T., Montgomery, J. A., Jr., Peralta, J. E., Ogliaro, F., Bearpark, M., Heyd, J. J., Brothers, E., Kudin, K. N., Staroverov, V. N., Kobayashi, R., Normand, J., Raghavachari, K., Rendell, A., Burant, J. C., Iyengar, S. S., Tomasi, J., Cossi, M., Rega, N., Millam, J. M., Klene, M., Knox, J. E., Cross, J. B., Bakken, V., Adamo, C., Jaramillo, J., Gomperts, R., Stratmann, R. E., Yazyev, O., Austin, A. J., Cammi, R., Pomelli, C., Ochterski, J. W., Martin, R. L., Morokuma, K., Zakrzewski, V. G., Voth, G. A., Salvador, P., Dannenberg, J. J., Dapprich, S., Daniels, A. D., Farkas, Ö., Foresman, J. B., Ortiz, J. V., Cioslowski, J., Fox, D. J., Gaussian 09, Revision A.02, Gaussian Inc., Wallingford CT, 2009.

Jaiswal, P., Jha, S. N., Borah, A., Gautam, A., Grewal, M. K., & Jindal, G., 2015, Detection and quantification of soymilk in cow–buffalo milk using Attenuated Total Reflectance Fourier Transform Infrared spectroscopy (ATR–FTIR), *Food chemistry*, 168, 41-47.

James, B., Williams, R., 1961, The oxidation–reduction potentials of some copper complexes, *Journal of the Chemical Society*, 2007-2019.

Janin, Y. L., 2007, Antituberculosis drugs: ten years of research, *Bioorganic & medicinal chemistry*, 15(7), 2479-2513.

Jmol: An open-source Java viewer for chemical structures in 3D, version 13.0, 2018, http://www.jmol.org/.

Kavan, L., Kastner, J., 1999, Raman and infrared spectroscopy Carbyne and carbynoid structures, *Springer*, 343-356.

Keresztury, G., & Jalsovszky, G., 1971, An alternative calculation of the vibrational potential energy distribution, *Journal of Molecular Structure*, 10(2), 304-305.

Kerker, M., 2016, The scattering of light and other electromagnetic radiation, *Elsevier*.

Larkin, P., 2017, Infrared and Raman spectroscopy: principles and spectral interpretation, *Elsevier*.

Larsen, P. E., 2016, Hollow MEMS: An integrated sensor for combined density, viscosity, buoyant mass and IR absorption spectrometry, *DTU Nanotech*.

Le Roy, R. J., 2017, RKR1: a computer program implementing the first-order RKR method for determining diatomic molecule potential energy functions, *Journal of Quantitative Spectroscopy and Radiative Transfer*, 186, 158-166.

Lokhov, A. V., Titov, N. A., 2016, Anharmonicity of internal atomic oscillation and effective antineutrino mass evaluation from gaseous molecular tritium β-decay, *Journal of Physics G: Nuclear and Particle Physics*, 43(7), 075102.

Martin, J.M.L., Alsenoy, C.V., Gar2PED, University of Antwerp, Antiwerp, 1995.

Pulay, P., T’drilk, F., 1967, *Acta Chim. Acad. Sci. Hung*, 52, 49.

Richings, G., Polyak, I., Spinlove, K., Worth, G., Burghardt, I., Lasorne, B., 2015, Quantum dynamics simulations using Gaussian wavepackets: the vMCG method, *International Reviews in Physical Chemistry*, 34(2), 269-308.

Roos, B. O., Lindh, R., Malmqvist, P. Å., Veryazov, V., Widmark, P. O., 2016, Basis Sets, *Multiconfigurational Quantum Chemistry*, 69-84.

Sathyanarayana, D. N., 2015, Vibrational spectroscopy: theory and applications, New Age International.

Scholkmann, F., Kleiser, S., Metz, A. J., Zimmermann, R., Pavia, J. M., Wolf, U., Wolf, M., 2014, A review on continuous wave functional near-infrared spectroscopy and imaging instrumentation and methodology, *Neuroimage,* 85, 6-27.

Shastri, A., Das, A. K., Krishnakumar, S., Singh, P. J., Raja Sekhar, B.N., 2017, Spectroscopy of N, N-dimethylformamide in the VUV and IR regions: Experimental and computational studies. *The Journal of chemical physics*, 147(22), 224305.

Umar, A., Oberacker, V., Simenel, C., 2015, Shape evolution and collective dynamics of quasifission in the time-dependent Hartree-Fock approach, *Physical Review C*, 92(2), 024621.

Wu, T., Shum, P. P., Shao, X., Huang, T., Sun, Y., 2014, Third harmonic generation from mid-IR to near-IR regions in a phase-matched silicon-silicon-nanocrystal hybrid plasmonic waveguide., *Optics Express*, 22(20), 24367-24377.

Yang, H., Yang, S., Kong, J., Dong, A., Yu, S., 2015, Obtaining information about protein secondary structures in aqueous solution using Fourier transform IR spectroscopy, *Nature protocols*, 10(3), 382.

Yilmaz, A., Bolukbasi, O., 2016, Molecular structure and vibrational spectroscopic studies of prothionamide by density functional theory, *Spectrochimica Acta Part A: Molecular and Biomolecular Spectroscopy*, 152, 262-271.

Zhou, J., Wang, Y., Liao, C., Sun, B., He, J., Yin, G., Zhong, X., 2015, Intensity modulated refractive index sensor based on optical fiber Michelson interferometer, *Sensors and Actuators B: Chemical*, 208, 315-319.

Zimmerman, P. M., Smereka, P., 2016, Optimizing vibrational coordinates to modulate intermode coupling., *Journal of chemical theory and computation*, 12(4), 1883-1891.

CURRICULUM VITAE

Personal Information	
Name Surname	Somaeia Adarrat
Place of Birth	Libya Misorata
Date of Birth	01.01 1988
Nationality	☐ T.C. ☐ Other: Libyan
Phone Number	05547032067
Email	salamaliali32@gmail.com
Web Page	

Educational Information	
B. Sc.	
University	Misurata University
Faculty	Engineering
Department	Physics Engineering
Graduation Year	2010

M. Sc.	
University	İstanbul University
Institute	Institute Of Graduate Studıes In Science And Engineering
Department	Physics
Programme	Physics